

Non-equilibrium sedimentation of colloids: confocal microscopy and Brownian dynamics simulations

Matthias Schmidt^{1,2}, C Patrick Royall³, Alfons van Blaaderen⁴ and Joachim Dzubiella⁵

¹ Theoretische Physik II, Universität Bayreuth, Universitätsstraße 30, D-95440 Bayreuth, Germany

² H H Wills Physics Laboratory, University of Bristol, Tyndall Avenue, Bristol BS8 1TL, UK

³ The School of Chemistry, University of Bristol, Bristol BS8 1TS, UK

⁴ Soft Condensed Matter, Debye Institute, Utrecht University, Princetonplein 5, 3584CC, Utrecht, The Netherlands

⁵ Physics Department (T37), Technical University Munich, James Franck Straße, D-85748 Garching, Germany

Received 10 August 2008, in final form 6 October 2008

Published 12 November 2008

Online at stacks.iop.org/JPhysCM/20/494222

Abstract

Experimental and computational details are presented for an investigation of the transient time evolution of colloidal dispersions confined in a horizontal slit pore and under the influence of gravity (Royall *et al* 2007 *Phys. Rev. Lett.* **98** 188304). We demonstrate that the interparticle interactions can be well described by those of effective hard spheres by comparing experimental results for the pair distribution function obtained in the homogeneous part of the settling system to the theoretical result for hard spheres in equilibrium. Using an effective hard sphere diameter that is 10% larger than that obtained by static light scattering takes account of the (screened) electrostatic repulsion between particles. As a simple computational model, we use Brownian dynamics computer simulations with hard sphere pair interactions and investigate the time evolution of the one-body density profile during sedimentation. We show that an ‘intrinsic clock’, that ticks only when trial moves are accepted, facilitates high accuracy of the time evolution of the density profile, even when using relatively large integration time steps for the Langevin equations of motion.

1. Introduction

A colloidal dispersion will reach equilibrium between sedimentation and diffusion when it is left undisturbed for a sufficient amount of time; a density gradient of the particles as a function of height results. The systematic study of such density profiles dates back to at least the work of Perrin [1]. Equilibrium sedimentation profiles of concentrated suspensions of colloids can be measured by a variety of means, including via the intensity of the depolarized light scattered by optically anisotropic particles [2], as recently applied to systems with hard-core repulsion and very short-ranged attractive forces between colloids [3].

Quantitative understanding has been obtained from theoretical studies of simple model fluids such as hard spheres [4, 5]. Density-functional theory (DFT) [6, 7] as a particularly powerful tool to study inhomogeneous systems

in equilibrium has been used to study systems such as hard spheres (see e.g. [8]) and adhesive hard spheres [9, 10] under gravity and confined in a planar slit. Dynamical DFT (DDFT) [11–15] is a recent and promising generalization of DFT suitable for studying dynamical properties of system governed by diffusive motion, in particular on small length scales where interparticle correlations are important.

Many studies demonstrate that sedimentation continues to constitute an active area of research: the relaxation towards equilibrium in sedimentation of charged colloids in a gravitational field was investigated [16]; interfacial colloidal sedimentation equilibrium was studied using intensity-based confocal microscopy [17] and closure-based density-functional theory [18]; in a kinetic lattice gas the ageing dynamics and density relaxation lattice gases under gravity were investigated [19].

Hydrodynamic interactions between the particles, mediated by the flow of the solvent, play an important role in sedimentation [20–22], and confinement is known to have a strong influence on hydrodynamic interactions: anomalous behaviour of hydrodynamic interaction was found e.g. in quasi-two-dimensional suspensions [23–25], and screened hydrodynamic interactions in a narrow channel [26]. Steady-state sedimentation dynamics of spherical particles was studied when the system was confined between upright plates [27] and Brownian dynamics simulation of the final stage of sedimentation was considered in a soft sphere model [28].

Much interesting work was carried out in the non-Brownian regime of large particles, investigating long-range correlations in sedimentation [29], non-universal velocity fluctuations of sedimenting particles [30], and an effective gravitational temperature for sedimentation [31]. The computer simulation work by Padding and Louis using techniques that take solvent hydrodynamics into account has shed much light on the nature of hydrodynamic and Brownian fluctuations [32–34].

In recent work [35] we have investigated the non-equilibrium, transient sedimentation of micron-sized colloidal particles using confocal microscopy, Brownian dynamics simulations and DDFT. We obtained quantitative agreement from the respective approaches for the time evolution of the colloid density profile as a function of height: Brownian dynamics simulation results confirmed the high accuracy of the DDFT for hard spheres, using Rosenfeld’s fundamental measures approximation [36] for the excess free energy; both theory and simulations neglect hydrodynamic interactions. Obtaining reliable data from Brownian dynamics simulations for the transient (non-steady-state) time evolution is a non-trivial computational task. In order to increase the efficiency of the numerical scheme we used an ‘intrinsic clock’, which enabled us to use large time steps when integrating the equations of motion. The account of this method given in [35] is very brief; we supply a detailed description below.

Taking hydrodynamics into account in a phenomenological manner (via a density-dependent mobility [21]) gave quantitative agreement of the results from DDFT and experiment in the two different systems considered, albeit with a mismatch in timescales of about 20% in one of the cases. In both theory and simulations, the interparticle interactions were modelled as hard spheres. Here we present results for the measured pair distribution function, obtained from confocal microscopy data, in order to show that the dispersion indeed behaves as hard-sphere-like, with an effective hard sphere diameter that models the screened electrostatic repulsion between the colloids.

We also found [35] that in experiments an ‘inverted’ sample (where the system is prepared such that the colloids are initially agglomerated at the top of the container and sediment downwards) displays a Rayleigh–Taylor-like instability. Similar behaviour has been reported on larger length scales in a sedimenting suspension of glass particles with diameters $> 50 \mu\text{m}$ inside a Hele–Shaw cell [37]. In computer simulations the instability of a fluid–fluid interface in driven colloidal mixtures when brought into non-equilibrium via a constant external driving field was investigated [38].

Recent work was aimed at further studying hydrodynamic instabilities in driven non-uniform colloidal dispersions [39].

The paper is organized as follows. In section 2 results from confocal microscopy are presented. Section 3 gives details about the novel method to carry out Brownian dynamics simulations of hard spheres. We conclude in section 4.

2. Confocal microscopy of settling dispersions

2.1. Experimental details

We used sterically stabilized, fluorescently labelled poly methyl methacrylate particles (PMMA) [40] with diameter of $\sigma = 2.8 \mu\text{m}$ and size polydispersity of around 0.05, both as determined from static light scattering. The particles were dispersed in a mixture of cyclohexyl bromide (CHB) and cis-decalin. We added $260 \mu\text{M}$ tetrabutyl ammonium bromide (TBAB) salt. This screens the (weak) electrostatic interactions between the colloids, resulting in hard sphere like behaviour, as demonstrated below. The (small) density difference between colloids and solvent controls the gravitational height $\xi_g = k_B T / (mg)$, where T is temperature, k_B is the Boltzmann constant, m is the buoyancy mass of the particles, and g is earth’s acceleration. The suspension was placed in a capillary, which was laid flat, so that the colloids sediment across the cell. Using confocal microscopy, the colloid coordinates were tracked in a time-resolved manner in three dimensions, as described in [41]. The coordinates were then analysed to obtain the particle density profile as a function of time and height. In the results shown below, the Peclet number $\text{Pe} \approx 1.11$ [35], where the Peclet number is obtained as the ratio of the particle radius and the gravitational height, $\text{Pe} = \sigma / (2\xi_g)$.

2.2. Confocal microscopy results

Figure 1 illustrates the process of sedimentation by displaying particle configurations at four different times during the sedimentation process. These images are renderings of particle coordinates obtained from confocal microscopy. The particles were initially dispersed homogeneously throughout the system. They sedimented downwards in the course of time. The natural timescale is formed by the Brownian time $\tau_B = 3\pi\eta\sigma^3 / (4k_B T)$ which it takes a particle to diffuse over its radius $\sigma/2$, with η denoting the shear viscosity of the solvent. At late times the bottom of the sediment became dense, but we did not find any indications of crystallization [35].

In order to characterize the type of pair interactions in the system we display results for the pair distribution function $g(r)$ in figure 2. We have obtained $g(r)$ from analysing the experimentally determined particle coordinates [41], at a relatively early time in the sedimentation experiment. The system is at this stage out of equilibrium. However, [32] shows that for $\text{Pe} \sim 1$ the local structure is little disturbed by the settling. We compare the experimental data for $g(r)$ to results obtained from Percus–Yevick theory for a bulk system in equilibrium, both using the bare particle diameter σ and packing fraction $\phi_0 = 0.142$, as well as a modified (larger) effective diameter $\sigma_{\text{eff}} = 1.1\sigma$ and consistently increased effective packing fraction $\phi_{0,\text{eff}} = (\sigma_{\text{eff}}/\sigma)^3 \phi_0 = 0.189$.

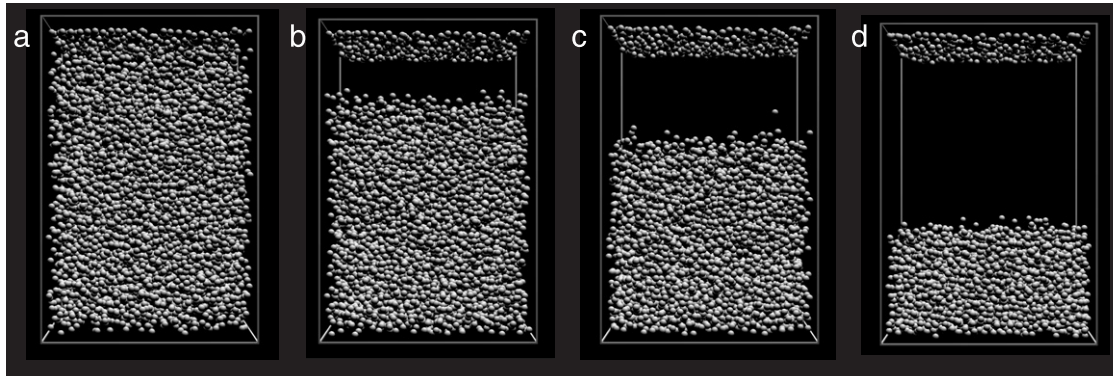


Figure 1. Computer generated representation of experimental results for the position coordinates of the colloidal particles in a sedimenting dispersion. The coordinates are obtained from analysing confocal scanning laser microscopy images at times $t/\tau_B = 28$ (a), 46 (b), 65 (c), and 255 (d). In (b)–(d), a layer of particles adsorbed to the top wall of the capillary is seen; these particles appear immobile.

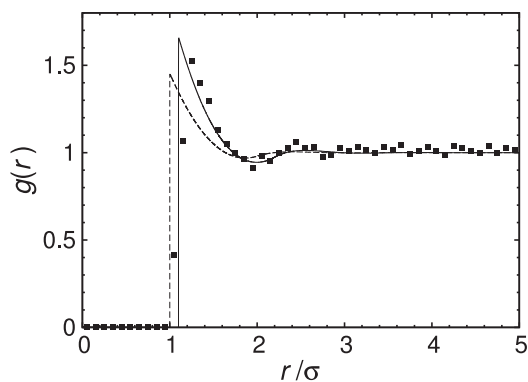


Figure 2. Experimental (symbols) and theoretical (lines) results for the pair distribution function $g(r)$ as a function of the scaled distance r/σ . The dashed line represents the result using the bare hard sphere diameter and packing fraction $\phi_0 = 0.142$; the full line is obtained using an effective (larger) hard sphere diameter $\sigma_{\text{eff}} = 1.1\sigma$ and effective packing fraction $\phi_{0,\text{eff}} = (\sigma_{\text{eff}}/\sigma)\phi_0 = 0.189$ in order to account for the screened electrostatic repulsion between the particles.

Using the latter parameters gives good agreement between experimental and theoretical results. The magnitude of the effective diameter is consistent with the value of the order of 100 nm for the Debye screening length [41, 42]. We conclude that the pair interactions in the system can be well represented by the hard sphere model.

Figure 3(a) shows (scaled) sedimentation profiles $\phi(z) = \pi\sigma^3\rho(z)/6$ determined from experiment, where $\rho(z)$ is the height-dependent density profile (recall that σ is the bare hard sphere diameter). Results at two different times are shown, $t = 46$ and $520 \tau_B$. For a more extensive discussion of the evolution of the sedimentation profile, the reader is referred to [35]. Here we note that in this regime of $Pe \sim 1$ the top of the profile displays a clear interface to a practically particle-free supernatant. We see further that the top of the profile is somewhat more extended at early times ($t = 46\tau_B$) than at later times ($t = 520\tau_B$). Motivated by this observation, we quantify the interfacial region by determining the positions z_1 and z_2 at which the density profile reaches, say, 20% and 80% respectively of the initial value in the homogeneous sample,

i.e.,

$$\phi(z_1) = 0.2\phi_0, \quad \phi(z_2) = 0.8\phi_0. \quad (1)$$

Using the heights z_1 and z_2 , the interface can be characterized by its position, obtained as the mean $z_0 = (z_1 + z_2)/2$, and by its width, obtained as the difference $\xi = z_1 - z_2$.

At early times (e.g. $t = 46\tau_B$, figure 3(a)), three different regions can be identified in the sedimentation profile: at the bottom, a dense region ($\phi > \phi_0$), in the middle, a region whose colloid volume fraction remains close to ϕ_0 , and the top, where $\phi \sim 0$. The value of z_0 serves to indicate the position of the interface between the middle and top regions. We plot the variation of z_0 with time t in figure 3(b) and find that z_0 is indeed initially linear in t , until, around $t = 100\tau_B$, there is a rather abrupt slowing down in the fall of $z_0(t)$. This corresponds to the ‘coalescence’ of the ‘interfacial’ region with the dense sediment. The intermediate $\phi \approx \phi_0$ region is thus absorbed into the sediment at the bottom. We argue that for $t > 100\tau_B$, at least compared to the initial conditions, the system is quite close to sedimentation equilibrium. Further compaction of the sediment might occur on a much longer timescale. Despite the confinement and coupling of length scales, such as the gravitational length ξ_g and σ , this local particle-level approach shows initial behaviour reminiscent of batch settling [43]. See also [43] for a discussion of the shape of kinetic sedimentation profiles on macroscopic scales.

The variation of the interfacial width ξ with time t is plotted in figure 3(c). We observe a clear change, again, at $t \approx 100\tau_B$. It appears that the initial stages of sedimentation may be seen almost as a steady-state non-equilibrium system, at least in the vicinity of z_0 . This steady-state regime ends rather abruptly at $t \approx 100\tau_B$ when z_0 becomes comparable to the height of the dense compacted sediment.

3. Brownian dynamics computer simulations

3.1. Langevin equations of motion

In our simulations the dynamics of the colloids is modelled as completely overdamped Brownian motion neglecting solvent-mediated hydrodynamic interactions between the particles. The stochastic Langevin equations for the colloidal trajectories

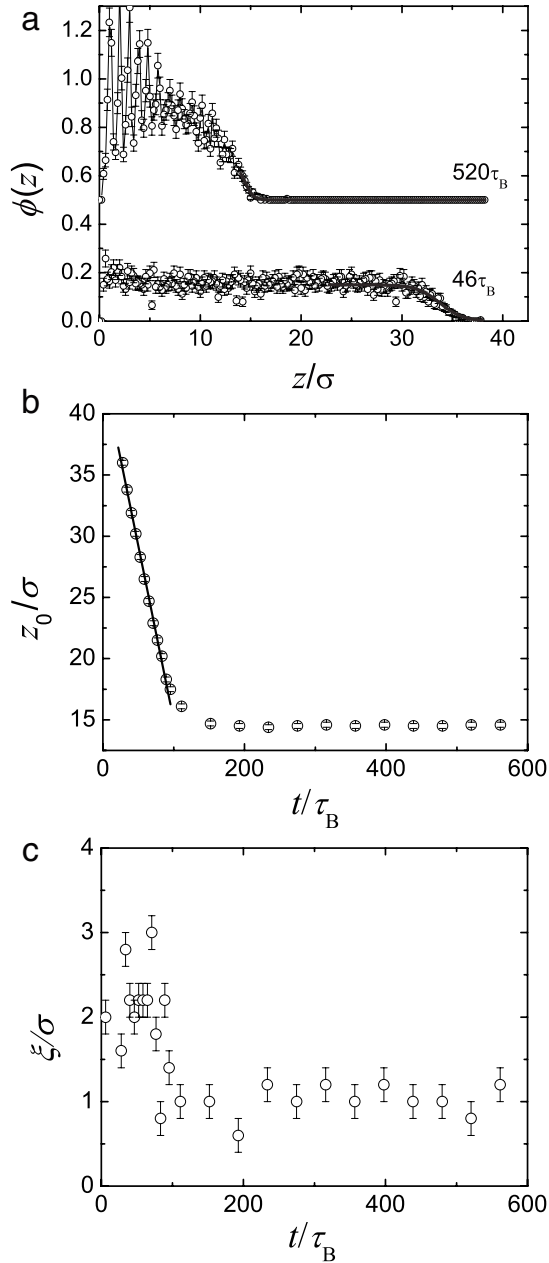


Figure 3. Results from confocal microscopy of a sedimenting dispersion. (a) The local packing fraction $\phi(z, t) = \rho(z, t)\pi\sigma^3/6$ as a function of the (scaled) height coordinate z/σ for (scaled) times $t/\tau_B = 46, 520$ (as indicated). The result for the later time is vertically offset by 0.5 for clarity. (b) The position z_0 of the interface between dispersion and supernatant as a function of time. A straight line fit yields a sedimentation velocity of $0.28\sigma\tau_B^{-1}$, while we expect a sedimentation velocity of $0.25\sigma\tau_B^{-1}$ from the Hayakawa–Ichiki expression for the mobility at a colloid volume fraction of $\phi_0 = 0.142$. (c) The time evolution of the interfacial width ξ .

$\mathbf{r}_i(t)$ where $i = 1, \dots, N$ labels the particles, and N is the total number of particles, read therefore as

$$\Gamma_0^{-1} \frac{d\mathbf{r}_i}{dt} = -\nabla_{\mathbf{r}_i} \sum_{i \neq j} V_{\text{HS}}(|\mathbf{r}_i - \mathbf{r}_j|) + \mathbf{F}_{\text{ext}} + \mathbf{F}_i^{(\text{R})}(t), \quad (2)$$

where $\Gamma_0^{-1} = 3\pi\eta\sigma$ is the friction constant. There are three different types of forces acting on the particles: the first term on the right-hand side of (2) is the force stemming from the interparticle (hard sphere) interactions V_{HS} , the second term represents both the external gravitational field and confinement by the (hard) walls at the bottom and at the top of the system $\mathbf{F}_{\text{ext}} = k_B T/\xi_g \mathbf{e}_z + \mathbf{F}_{\text{walls}}$; the third term is a random force $\mathbf{F}_i^{(\text{R})}(t)$ arising from kicks of the solvent molecules on the i th colloidal particle. These kicks are Gaussian random variables with zero mean, $\overline{\mathbf{F}_i^{(\text{R})}} = 0$, and variance

$$\overline{(\mathbf{F}_i^{(\text{R})})_\alpha(t)(\mathbf{F}_j^{(\text{R})})_\beta(t')} = 2k_B T \Gamma_0^{-1} \delta_{\alpha\beta} \delta_{ij} \delta(t - t'). \quad (3)$$

The subscripts $\alpha, \beta = 1, 2, 3$ enumerate the Cartesian components. We solved the Langevin equations of motion (2) numerically using a finite time step Δt and the technique of Ermak [44].

3.2. Intrinsic clock versus external time

It was recognized almost two decades ago that the use of hard-core interactions $V_{\text{HS}}(r)$ in Brownian dynamics simulations is problematic, as the interparticle forces are singular at contact [45, 46]. To resolve this problem Cichocki and Hinsen (CH) proposed a method in which particle overlaps are avoided by introducing a Monte Carlo (MC) like trial and rejection scheme. In this procedure, however, *dynamical properties* depend strongly and systematically on the magnitude of the numerical integration time step Δt . CH resorted to extrapolating their results to the limit $\Delta t \rightarrow 0$. This requires carrying out simulation using a range of different time steps, increasing computational demands. Several improvements and conceptually different methods have been proposed to address this problem, e.g. by correcting overlaps geometrically [47] or treating collisions elastically [48]. Other more recent attempts to rescale the Brownian dynamics simulated properties by comparing to dynamically equivalent soft sphere systems [49], or approximate overlaps by the analytical two-body Smoluchowski equation [50].

In our Brownian dynamics simulation of the non-equilibrium time evolution of hard spheres we reconsider the original MC-like scheme of CH and show that a minor supplement to their method allows us to calculate accurate density profiles efficiently by employing relatively large integration time steps. In the CH method, each of the N particles subsequently performs a trial move during one integration time step of duration Δt , so that the time passed during updating a single particle is $\Delta t/N$. After n time steps (updates of all N particles) a time $t = n\Delta t$ has passed, which we in the following refer to as the ‘external time’. This time also proceeds when particles are not moved, even in the case where no particle has moved in a trial cycle during time Δt . For large time steps and dense systems this obviously leads to large errors in the timescale of particle motion, as numerous many-body overlaps naturally occur, collective motions are forbidden, and consequently the systems becomes almost immobile although the time ticks. As we empirically find, a simple fix of this problem is to advance time *only* if a

particle moves. For instance, if in one time step (of duration Δt) 30% of the N trial moves are accepted, only the time $t_i = 0.3\Delta t$ has passed. In general, let $\chi(t)$ be the fraction of successful particle moves from time t to $t + \Delta t$; then summing over time steps yields $t_i = \sum_{t'=0}^t \chi(t')\Delta t$. We refer to t_i in the following as the ‘intrinsic time’, measured by an ‘intrinsic clock’ that ticks regularly, but in variable intervals of length $\chi(t)\Delta t$. We illustrate and validate this procedure in the following by displaying selected simulation results.

We consider hard spheres in a gravitational field of strength $\sigma/\xi_g = 1.32$ confined between two walls separated at a distance $L = 11.43\sigma$. The vertically integrated density is equivalent to the number of particles per unit lateral area and is chosen to be $\int_0^L dz \rho(z) = 4.0\sigma^{-2}$, corresponding to an average packing fraction of $\phi_0 = \frac{\pi\sigma^3}{6L} \int_0^L dz \rho(z) = 0.1832$. We perform Brownian dynamics simulations with five different time steps $\Delta t = 0.0005, 0.001, 0.025, 0.01, 0.02\tau_B$ (using periodic boundary conditions in the directions perpendicular to gravity) and measure the non-equilibrium density profiles at certain times t , as shown in figure 4 for $t = 1.5$ and $3.5\tau_B$. We start from an initially homogeneous profile $\rho(z) = 6\phi_0/(\pi\sigma^3)$ and the particles sediment towards negative z -values in the course of time. We find that the rejection probability on time average (over the whole run) increases with magnitude of the time step, as would be intuitively expected, and is 15%, 22%, 33%, 52%, and 60% for the time steps given above, respectively (note that the rejection probability is t dependent in general as the density inhomogeneity changes in time). As observed by CH, only by extrapolating $\Delta t \rightarrow 0$ the dynamic behaviour is accurately obtained. The dependence of the rejection rate on the magnitude of the time step further implies that the intrinsic clock ticks more slowly compared to the external time as we increase Δt , and the profiles measured at external time t are retarded. This systematic error is illustrated in the inset of figure 4 for $t = 3.5\tau_B$: it can be observed clearly that for large values of Δt the profiles are not as far relaxed as in the limit to vanishing time steps $\Delta t \rightarrow 0$. In the main plot, we show the density profiles according to the intrinsic time t_i : all curves overlap on a master curve with hardly any difference in structure. We find that the result for $\Delta t = 0.0005\tau_B$ is indistinguishable from the CH extrapolation procedure, indicating that our procedure works within acceptable error. We have also tested this proposal for other parameters and always found only very minor dependence on the magnitude of the time step.

The major advantage of the intrinsic clock is that it allows us to calculate accurately *non-equilibrium* structures using relatively large time steps. The numerical effort is low as the same MC-like integration scheme as originally proposed by CH is employed—only the interpretation of the ‘numerical time’ is different. Whether this procedure is helpful to efficiently calculate further dynamical properties, such as diffusion constants or the viscosity [48], remains to be tested.

4. Conclusions and outlook

Via analysing data for the pair distribution function we have shown that the system investigated in [35] possesses

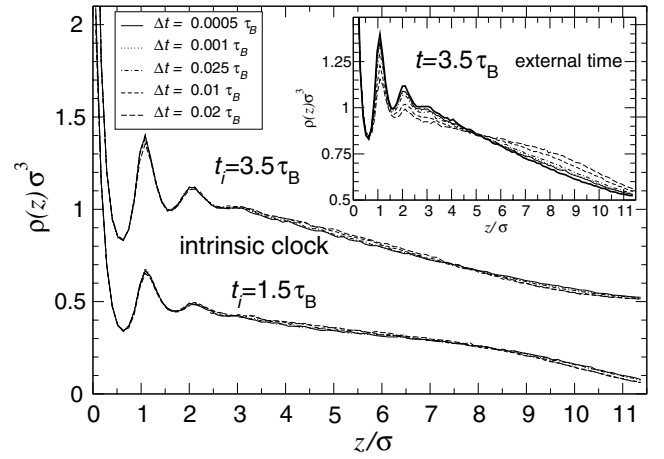


Figure 4. Non-equilibrium density profiles $\rho(z)\sigma^3$ of hard spheres with diameter σ in a gravitational field along the z -direction, calculated by Brownian dynamics computer simulations. Parameters are $L = 11.43\sigma$, $\xi_g = 0.76\sigma$, and $\phi_0 = 0.1832$. Profiles are shown for two different times $t = 1.5$ and $3.5\tau_B$ (shifted upward by 0.5 units) during sedimentation where t is measured by the ‘intrinsic clock’; see the main text. Comparing the results using different integration time steps ranging from 0.0005 to $0.02\tau_B$ shows hardly any difference. Inset: $\rho(z)\sigma^3$ at $t = 3.5\tau_B$ but measured with the external time. The deviation and error with larger integration time steps in Brownian dynamics becomes obvious. The thick solid curve is the extrapolated curve from the CH method ($\Delta t \rightarrow 0$) as a reference. This is hardly distinguishable from the result obtained using the intrinsic clock and $\Delta t = 0.0005$.

hard-sphere-like interactions, and that the initial stages of sedimentation appear to have steady-state like characteristics at the ‘top’ of the sediment, in other words that the behaviour even of this strongly confined system is reasonably consistent with batch settling. Details of the ‘intrinsic clock’ simulation technique for Brownian dynamics of hard spheres have been given.

It is worth mentioning that recent work was devoted to extending and complementing the DDFT used in [35], e.g. considering the one-dimensional asymmetric exclusion process [51], using a dynamical test particle limit in order to calculate two-body dynamic (van Hove) correlation functions [52], investigating particles in a flowing solvent [53], as well as treating atomic systems [54].

Further interesting questions arise from relating our work to crystallization of colloidal hard spheres under gravity [55, 56] and dynamic broadening of the crystal–fluid interface of colloidal hard spheres [57], as well as the competition between sedimentation and phase separation [58].

Acknowledgments

We thank A J Archer, S Buzzaccaro, D Derks, Y Levin, H Löwen, J F Nye, R Piazza, H Tanaka, and A Wysocki for inspiring discussions, H Tanaka for microscope time and D Derks for particle synthesis. JD thanks the *Deutsche Forschungsgemeinschaft* for support via the Emmy Noether Programme. CPR gratefully acknowledges the Royal Society for financial support. This work is part of the

Stichting voor Fundamenteel Onderzoek der Materie (FOM), which is supported by the Nederlandse Organisatie voor Wetenschappelijk Onderzoek (NWO).

References

- [1] Perrin J 1910 *J. Physique* **9** 5
- [2] Piazza R, Bellini T and Degiorgio V 1993 *Phys. Rev. Lett.* **71** 4267
- [3] Buzzaccaro S, Rusconi R and Piazza R 2007 *Phys. Rev. Lett.* **99** 098301
- [4] Biben T, Hansen J P and Barrat J L 1993 *J. Chem. Phys.* **98** 7330
- [5] Biben T and Hansen J 1994 *J. Phys.: Condens. Matter* **6** A354
- [6] Evans R 1979 *Adv. Phys.* **28** 143
- [7] Evans R 1992 *Fundamentals of Inhomogeneous Fluids* ed D Henderson (New York: Dekker) chapter 3, p 85
- [8] Chen H and Ma H 2006 *J. Chem. Phys.* **125** 024510
- [9] Jamnik A 1998 *J. Chem. Phys.* **109** 11085
- [10] Choudhury N and Ghosh S K 2002 *J. Chem. Phys.* **116** 384
- [11] Marini Bettolo Marconi U and Tarazona P 1999 *J. Chem. Phys.* **110** 8032
- [12] Marini Bettolo Marconi U and Tarazona P 2000 *J. Phys.: Condens. Matter* **12** A413
- [13] Dzubiella J and Likos C N 2003 *J. Phys.: Condens. Matter* **15** L147
- [14] Archer A J and Evans R 2004 *J. Chem. Phys.* **121** 4246
- [15] Archer A J and Rauscher M 2004 *J. Phys. A: Math. Gen.* **37** 9325
- [16] Dufreche J F, Simonin J P and Turq P 1999 *J. Mol. Liq.* **79** 137
- [17] Beckham R E and Bevan M A 2007 *J. Chem. Phys.* **127** 164708
- [18] Lu M, Bevan M A and Ford D M 2007 *J. Chem. Phys.* **127** 164709
- [19] Levin Y, Arenzon J J and Sellitto M 2001 *Europhys. Lett.* **55** 767
- [20] Cichocki B and Felderhof B U 1989 *Physica A* **154** 213
- [21] Hayakawa H and Ichiki K 1995 *Phys. Rev. E* **51** R3815
- [22] Felderhof B U 2002 *J. Stat. Phys.* **109** 482
- [23] Cui B, Diamant H, Lin B and Rice S A 2004 *Phys. Rev. Lett.* **92** 258301
- [24] Diamant H, Cui B, Lin B and Rice S A 2005 *J. Phys.: Condens. Matter* **17** S2787
- [25] Diamant H, Cui B, Lin B and Rice S A 2005 *J. Phys.: Condens. Matter* **17** S4047
- [26] Cui B, Diamant H and Lin B 2002 *Phys. Rev. Lett.* **89** 188302
- [27] Kuusela E, Lahtinen J M and Ala-Nissila T 2004 *Phys. Rev. E* **69** 066310
- [28] Nuesser W and Versmold H 1999 *Mol. Phys.* **96** 893
- [29] Segre P N, Herbolzheimer E and Chaikin P M 1997 *Phys. Rev. Lett.* **79** 2574
- [30] Tee S Y, Mucha P J, Cipelletti L, Manley S, Brenner M P, Segre P N and Weitz D A 2002 *Phys. Rev. Lett.* **89** 054501
- [31] Segre P N, Liu F, Umbanhowar P and Weitz D A 2001 *Nature* **409** 594
- [32] Padding J T and Louis A A 2004 *Phys. Rev. Lett.* **93** 220601
- [33] Padding J T and Louis A A 2006 *Phys. Rev. E* **74** 031402
- [34] Padding J T and Louis A A 2008 *Phys. Rev. E* **77** 011402
- [35] Royall C P, Dzubiella J, Schmidt M and van Blaaderen A 2007 *Phys. Rev. Lett.* **98** 188304
- [36] Rosenfeld Y 1989 *Phys. Rev. Lett.* **63** 980
- [37] Völtz C, Pesch W and Rehberg I 2001 *Phys. Rev. E* **65** 011404
- [38] Wysocki A and Löwen H 2004 *J. Phys.: Condens. Matter* **16** 2709
- [39] Wysocki A, Royall C P, Winkler R G, Gompper G, Tanaka H, van Blaaderen A and Löwen H 2008 arXiv:0810.1258
- [40] Bosma G, Pathmanathan C, de Hoog E H A, Kegel W K, van Blaaderen A and Lekkerkerker H N W 2002 *J. Colloid Interface Sci.* **245** 292
- [41] Royall C P, Leunissen M E and van Blaaderen A 2003 *J. Phys.: Condens. Matter* **15** S3581
- [42] Yethiraj A and van Blaaderen A 2003 *Nature* **421** 513
- [43] Russel W B, Saville D A and Schowalter W R 1989 *Colloidal Dispersions* (Cambridge: Cambridge University Press)
- [44] Ermak D L 1975 *J. Chem. Phys.* **62** 4189
- [45] Cichocki B and Hinsen K 1990 *Physica A* **166** 473
- [46] Cichocki B and Hinsen K 1992 *Physica A* **187** 133
- [47] Schaertl W and Silesco H 1994 *J. Stat. Phys.* **74** 678
- [48] Strating P 1999 *Phys. Rev. E* **59** 2175
- [49] Guevara-Rodriguez F de J and Medina-Noyola M 2003 *Phys. Rev. E* **68** 011405
- [50] Scala A, Voigtmann T and De Michele C 2007 *J. Chem. Phys.* **126** 134109
- [51] Dwandaru W S B and Schmidt M 2007 *J. Phys. A: Math. Gen.* **40** 13209
- [52] Archer A J, Hopkins P and Schmidt M 2007 *Phys. Rev. E* **75** 040501(R)
- [53] Rauscher M, Dominguez A, Kruger M and Penna F 2007 *J. Chem. Phys.* **127** 244906
- [54] Archer A J 2006 *J. Phys.: Condens. Matter* **18** 5617
- [55] Marechal M and Dijkstra M 2007 *Phys. Rev. E* **75** 061404
- [56] Hoogenboom J P, Vergeer P and van Blaaderen A 2003 *J. Chem. Phys.* **119** 3371
- [57] Dullens R P A, Aarts D G A L and Kegel W 2006 *Phys. Rev. Lett.* **97** 228301
- [58] Aarts D G A L, Dullens R P A and Lekkerkerker H N W 2005 *New J. Phys.* **7** 40